



OPEN

Odontogenesis-associated phosphoprotein truncation blocks ameloblast transition into maturation in *Odaph*^{C41*/C41*} mice

Tian Liang¹, Yuanyuan Hu¹, Kazuhiko Kawasaki³, Hong Zhang¹, Chuhua Zhang¹, Thomas L. Saunders², James P. Simmer^{1✉} & Jan C.-C. Hu¹

Mutations of Odontogenesis-Associated Phosphoprotein (*ODAPH*, OMIM *614829) cause autosomal recessive amelogenesis imperfecta, however, the function of *ODAPH* during amelogenesis is unknown. Here we characterized normal *Odaph* expression by in situ hybridization, generated *Odaph* truncation mice using CRISPR/Cas9 to replace the TGC codon encoding Cys41 into a TGA translation termination codon, and characterized and compared molar and incisor tooth formation in *Odaph*^{+/+}, *Odaph*^{+/C41*}, and *Odaph*^{C41*/C41*} mice. We also searched genomes to determine when *Odaph* first appeared phylogenetically. We determined that tooth development in *Odaph*^{+/+} and *Odaph*^{+/C41*} mice was indistinguishable in all respects, so the condition in mice is inherited in a recessive pattern, as it is in humans. *Odaph* is specifically expressed by ameloblasts starting with the onset of post-secretory transition and continues until mid-maturation. Based upon histological and ultrastructural analyses, we determined that the secretory stage of amelogenesis is not affected in *Odaph*^{C41*/C41*} mice. The enamel layer achieves a normal shape and contour, normal thickness, and normal rod decussation. The fundamental problem in *Odaph*^{C41*/C41*} mice starts during post-secretory transition, which fails to generate maturation stage ameloblasts. At the onset of what should be enamel maturation, a cyst forms that separates flattened ameloblasts from the enamel surface. The maturation stage fails completely.

C4orf26 (Chromosome 4 open reading frame 26) was unknown to enamel scientists until geneticists found pathogenic variants in the gene that caused autosomal recessive inherited enamel defects in humans^{1,2}. The six reported *ODAPH* pathogenic variants included two frameshifts [p.(Cys14Glyfs*21), p.(Val18Cysfs*23)], a splice junction mutation (c.68-2A>T), and three premature termination codons [p.(Cys43*), p.(Arg77*), and p.(Trp106*)]. *C4orf26* was found to be inactivated in toothless placental mammals, so its conservation by natural selection is restricted to its function³. Given this functional specificity, the gene designation was changed from *C4orf26* to *ODAPH* (Odontogenesis-Associated Phosphoprotein, OMIM *614829). Human *ODAPH* encodes a protein of 130 amino acids, including a 23 amino acid signal peptide and a secreted protein of 107 amino acids, which includes 19 prolines, 3 cysteines and multiple serines in context for phosphorylation by the Golgi Casein Kinase complex⁴. This kinase complex includes FAM20A⁵ and FAM20C⁶ and catalyzes functionally critical phosphorylations on three other secreted enamel matrix proteins: enamelin^{7,8}, ameloblastin⁹, and amelogenin¹⁰. In vitro studies showed phosphorylated *ODAPH* has the capacity to promote nucleation of hydroxyapatite¹.

Pharyngeal teeth called conodonts were the first tissues to mineralize in chordates/vertebrates, about 515 mya¹¹. They served as a feeding apparatus in an eel-shaped, jawless fish^{12,13}. Conodonts are analogous, but not homologous, to teeth in jaws¹⁴. Predation by conodonts may have helped drive the evolution of scales, some of which contained dentin, often topped with a thin hypomineralized layer of enamel or enameloid^{15,16}. Scales are

¹Department of Biologic and Materials Sciences, University of Michigan School of Dentistry, 1210 Eisenhower Place, Ann Arbor, MI 48108, USA. ²Department of Internal Medicine, Division of Molecular, Medicine and Genetics, University of Michigan Medical School, Ann Arbor, MI 48109, USA. ³Department of Anthropology, Pennsylvania State University, University Park, PA 16802, USA. ✉email: jsimmer@umich.edu

homologous to teeth, which evolved by the internalization of scales along with or shortly after the evolution of jaws¹⁷.

The evolution of bone, dentin, enameloid and enamel involved numerous duplications in SPARCL1 (SPARC Like 1), generating clusters of secretory calcium-binding phosphoprotein (SCPP) genes that mediate biomineralization^{18,19}. In the human genome, AMEL (amelogenin) is located on both Xp22.2 and Yp11.2²⁰. There are two large SCPP gene clusters on 4q13.3–4q22.1, one encoding 16 proline/glutamine-rich proteins, the other encoding 7 acidic proteins, including SPARCL1²¹. The two clusters are 17 Mb apart. Curiously, *ODAPH*, which is not an SCPP gene, is located in the 17 Mb region between the two clusters (4q21.1).

Dental enamel formation is divided into two main stages: secretory and maturation. During the secretory stage enamel ribbons initiate on the surface of dentin and elongate with continued enamel matrix secretion and assembly to establish the full thickness of the enamel layer. Disturbances to tooth formation that occur during the secretory stage generally reduce the thickness of the enamel layer, causing enamel hypoplasia²². Upon completion of the secretory stage, ameloblasts transition into the maturation stage and harden the enamel by growing the thin enamel ribbons deposited during the secretory stage in width and thickness, causing them to interlock^{23,24}. Disturbances to tooth formation that occur during the maturation stage generally cause enamel hypomineralization, reducing the hardness of the enamel layer²².

To advance our understanding of the role played by *ODAPH* during tooth formation, we characterized the expression of *Odaph* during mouse tooth development, generated and characterized *Odaph*^{C41*} knockin mice in the C57BL/6N background, and investigated the evolutionary history of the *Odaph* gene during vertebrate evolution. The Cys41* truncation in mouse is homologous to the p.(Cys43*) defect that caused autosomal recessive amelogenesis imperfecta in humans¹, and should the mutant transcript be expressed, the resulting secreted protein would be very short (18 amino acids) and unlikely to have biological activity.

Materials and methods

Regulatory compliance. The animal study protocol was reviewed and approved by the Institutional Animal Care and Use Committee at the University of Michigan and all experiments were performed in accordance with relevant guidelines and regulations.

Generation of the *Odaph* knockin mouse model. CRISPR/Cas9 technology was used to generate a genetically modified mouse strain carrying the mouse Odontogenesis Associated Phosphoprotein (*Odaph*, formerly *Gm1045*) gene modified by introduction of a translation termination codon (TGA) to replace the cysteine codon (TGC) at position 41. There is only one mRNA transcript variant for mouse *Odaph* (NCBI reference sequence NM_001177577.1). This codon change corresponds to a human *ODAPH* pathogenic variant c.129C>A; p.(Cys43*) that causes autosomal recessive amelogenesis imperfecta¹.

The following procedures were conducted by the University of Michigan Transgenic Animal Core. A single guide RNA (sgRNA) target and protospacer adjacent motif (PAM) were identified by a search of the mouse *Odaph* coding sequence in Exon 2 (101 bp, NM_001177577.1: nucleotides 65–165 starting from the translation initiation codon) using the CRISPR tool²⁵. The sgRNA target to direct Cas9 nuclease cleavage in the Cys41 codon was GAGGAGTGAGTGTGAAGATCTGG (Fig. S1). Ribonucleoprotein complexes of 30 ng/μL sgRNA + 30 ng/μL Cas9 protein were injected into fertilized mouse eggs by pronuclear microinjection to test for sgRNA induced Cas9 mediated chromosome breaks. Eggs were permitted to develop to the 64-cell blastocyst stage in vitro and then DNA was extracted from individual blastocysts for analysis. A PCR fragment spanning the expected Cas9 cut site was amplified and the product characterized by DNA sequence analysis. Small insertions/deletions (indels) caused by nonhomologous end joining repair of Cas9 mediated chromosome breaks were detected by the presence of multiple overlapping templates in the Sanger sequencing reaction. An ultramer DNA oligonucleotide donor was obtained from IDTDNA.com: TGGTTGGTGGTAACTACAGCAGAAGGACAAGATGTA GTCACCCCTCCTGGCGGCTCACAAAATAACGCAAAGCCTACcGAtTgAcAGATtTTtAcCtTgACTCCT CCGCCCACCACAAGGAATCTGGTAAACAAGGGCCAGCCCATCCCAAGGACACCCACGTTTTCTTTTT CCLower case letters indicate changes introduced to block sgRNA binding and Cas9 induced chromosome breaks after the oligonucleotide was incorporated into the chromosome by homology directed repair. These sequence changes were strategically introduced into the *Odaph* allele to eliminate a *Bgl*II restriction site and to generate a mutant-allele-specific primer annealing site to simplify genotyping. In the fertilized C57BL/6J eggs, homology directed repair of the chromosome replaced the homologous wild-type sequence with that of the symmetrical oligonucleotide donor. Fertilized eggs were produced by mating superovulated C57BL/6J female mice mated with C57BL/6J males (Jackson Laboratory Stock 000664). The genome editing reagent mixture for microinjection contained 30 ng/μL sgRNA + eSpCas9(1.1) protein (50 ng/μL) + oligonucleotide donor 10 ng/μL. After the microinjection, surviving eggs were transferred to B6D2F1 pseudopregnant recipients (Jackson Laboratory Stock 100006). DNA samples were collected for genotype analysis from the pups born after embryo transfer.

Germline transmission. Genotyping assays identified three female and two male G0 founder mice that carried the *Odaph* p.Cys41* mutation. The G0 founder mice were crossed with C57BL/6 N (Charles River, strain code 027) for two generations to dilute any possible off-target effect of the CRISPR/Cas9 gene editing and to generate offspring for characterization. All G0 founders demonstrated germline transmission. Neither the founders nor their offspring had observable changes in their behavior and no apparent physical defects from neonatal stage to young adulthood. Genotyping and sequence validation were conducted as described in Fig. S2.

***Odaph*^{C41*} genotyping and validation.** DNA collected from tail biopsies was amplified using *Odaph*-specific primers F: 5' ATTCTCCATAAAATCAGATTTGTGCTGA and R: 5'-AATGTGTAATCCAAACTC

CTTGTTGTTGA that generated a 996 bp amplification product in both the wild-type and mutant mice. The PCR conditions were 94 °C for 2 min, then 35 cycles of [94 °C for 30 s, 59 °C for 30 s, 72 °C for 30 s] followed by 72 °C for 60 s and then hold at 4 °C. Each PCR reaction contained 10 µL of Platinum Hot Start PCR Master Mix (2×) (Invitrogen, Carlsbad, CA, USA), 1 µL of 10 µM Primer mix, 3 µL of DNA (40–50 ng/µL) template and 6 µL distilled water. The reactions were run using a GeneAmp PCR System 9700 (Applied Biosystems, Foster City, CA, USA). The amplification products were restricted with *Bgl*II, which only cleaves the WT amplicon as a *Bgl*II site was eliminated by the CRISPR design. Each reaction contained 10 µL of PCR products (~0.2 µg), 2.5 µL of NEB buffer 3.1 (10×) and 0.6 µL of NEB *Bgl*II (New England Biolabs, Rowley, MA, USA) and raised to 25 µL with distilled water. The reactions were incubated at 37 °C for 30 min and loaded on 1.5% agarose gel. The *Odaph*^{C41*/C41*} amplicon was 996 bp; the restricted *Odaph*^{+/+} amplicon was 560 and 436 bp (Fig. S2A). The *Odaph*^{C41*/C41*} amplicon was characterized by DNA sequencing and showed no differences with the wild-type except those intended, which are shown in the DNA sequence chromatograms (Fig. S2B). All coding exons and exon–intron junctions of F1 mice were confirmed by Sanger sequencing. F1 mice with correctly targeted sequences were bred with B6 to generate F2 for colony expansion.

RNA was isolated from enamel organ epithelia (EOE) dissected from *Odaph*^{C41*/C41*} and *Odaph*^{+/+} first molars at D5 (secretory stage) and D11 (maturation stage) using a Dynabeads mRNA Direct Purification Kit (Invitrogen, Carlsbad, CA, USA), converted to cDNA by reverse transcription, PCR amplified using Platinum Hot Start PCR Master Mix (2×) (Invitrogen) and visualized on a 1.5% agarose gel. *Odaph*-specific primers F: 5'-GTGAGTGCTCAGGGCAGAA; R: 5'-CGGTCTCATTAATAATGTCCTTCA generated a 753 bp amplification product in both the wild-type and mutant. The PCR conditions were 94 °C for 2 min, then 28 cycles of [94 °C for 30 s, 58 °C for 30 s] followed by 72 °C for 60 s. A similar amplification was run using *Gapdh*-specific primers F: 5'-AGGCCG GTGCTGAGTATGTC; R: 5'-TGCCTGCTTACCACCTTCT that generated a 530 bp amplification product.

Dissecting microscopy. Seven-week-old *Odaph*^{+/+}, *Odaph*^{+/C41*}, and *Odaph*^{C41*/C41*} mice were lightly anesthetized with isoflurane and their frontal facial images were taken using a dissection microscope. At least three samples from each genotype were assessed. A separate group of mice were deeply anesthetized with isoflurane and perfused with 1× phosphate buffered saline (PBS) for 10 min. Their mandibles were dissected and denuded of soft tissues, post-fixed by immersion in 4% paraformaldehyde (PFA) overnight, and rinsed with PBS three times, for 5 min each. The teeth were cleaned with 1% bleach (sodium hypochlorite), rinsed with PBS, air dried, displayed on the Nikon SMZ1000 dissection microscope, and photographed using a Nikon DXM1200 digital camera, as described previously²⁶.

In situ hybridization. Mandibles containing developing incisors were harvested from wild-type C57BL/6 N mice at 7-weeks, formalin-fixed, decalcified in a solution of 150 mM NaCl/10% acetic acid, paraffin embedded, microtome sectioned, and deparaffinized in xylene. An antisense *Odaph* RNA probe for RNAscope in situ hybridization was designed and produced by Advanced Cell Diagnostics (Newark, CA, USA). RNAscope 2.5 Assay with RED HD Detection Reagent (Advanced Cell Diagnostics, Inc. Newark, CA, USA) was performed for in situ hybridization, following user manual 322452 (FFPE sample preparation and pretreatment) and 322360 (RNAscope 2.5 HD Detection Reagent – RED user manual) provided by the manufacturer, as described previously²⁷. The following probes were used: (1) Mm-*Odaph* (Cat #576061, targeting NM_01177577.1, nt 2-743); (2) Mm-*Klk4* (Cat #483451, targeting NM_019928.1, nt 235-1228); and (3) Neg Ctrl Probe_dapB (Cat #310043). Photographs were taken using a Nikon Eclipse TE300 microscope equipped with a Nikon DXM1200 digital camera.

Histological analysis. Heads of *Odaph*^{+/+}, *Odaph*^{+/C41*}, and *Odaph*^{C41*/C41*} mice at postnatal days 5, 8 and 12 were harvested and the mandibles were dissected from the heads. Samples were fixed in 4% paraformaldehyde in diethyl pyrocarbonate (DEPC)-treated phosphate buffered saline (PBS; 137 mM NaCl, 2.7 mM KCl, and 11.9 mM phosphates) at 4 °C overnight (~18 h). The samples were decalcified in DEPC-treated 4.13% disodium ethylenediaminetetraacetic acid (EDTA, pH 7.4) at 4 °C with agitation, with the EDTA solution changed every 3 days for 5 to 12 days, depending on the ages. The samples were then dehydrated and embedded in paraffin. Mesial-distal sections (5 µm) were prepared for histological analysis. Hematoxylin and Eosin (H&E) staining was described previously²⁶. Photos were taken using a Nikon Eclipse TE300 microscope, and photographed using a Nikon DXM1200 digital camera.

Backscattered scanning electron microscopy (bSEM). Whole surface scanning was performed on 7-week-old molars of *Odaph*^{+/+}, *Odaph*^{+/C41*}, and *Odaph*^{C41*/C41*} hemi-mandibles. Hemi-mandibles were submerged in 4% PFA overnight and on the following day were carefully dissected of soft tissues, submerged in 1% NaClO for 20 min, rinsed, dehydrated using an acetone series (30, 50, 70, 80, 90, and 100%) and air dried. The hemi-mandibles were mounted on metallic stubs using conductive carbon cement, and imaged using a Joel JSM-7800FLV field-emission scanning electron microscope operating at an accelerating voltage of 15 kV in the backscatter mode at the University of Michigan Robert B. Mitchell Electron Microbeam Analysis Lab (EMAL, Ann Arbor, MI, USA).

Mouse incisors and molars were prepared for bSEM characterization following an optimized protocol²⁸. Seven-week-old *Odaph*^{+/+}, *Odaph*^{+/C41*}, and *Odaph*^{C41*/C41*} mice were anesthetized with isoflurane, perfused with 4% PFA, dissected free of soft tissue, dehydrated with an acetone series (30, 50, 70, 80, 90, and 100%), embedded in epoxy, and cross sectioned at 1 mm increments along their lengths as described previously^{29,30}. Wild-type incisor cross sections at Level 8 align with the buccal crest of alveolar bone and show fully formed enamel that has not yet erupted into the oral cavity. The polished cut surface was coated with carbon to increase conductivity

and examined at $\times 5000$ magnification in Joel 7800 (JEOL USA, Inc., Peabody, MA, USA) using the backscatter mode at a beam current of 20 kV and 10 nA. Images were captured at a working distance of 10 mm, with minor adjustments to focus. Selected images were normalized to have the same mean grayscale intensities for mineralized dentin using ImageJ (<http://rsb.info.nih.gov/ij/>), so that the grayscale of bSEM images from different images would most accurately be compared for degree of mineralization (whiter = higher mineralization).

Identification of *Odaph* orthologs. *Odaph* orthologs were identified in the window of human *Odaph* at the UCSC genome browser (<http://genome.ucsc.edu/index.html>) using the conservation track. For non-eutherian orthologs, which show limited sequence identities at the nucleotide level, genomic regions syntenic to human *Odaph* was investigated (downstream of *Cdckl2*), and intron spanning RNA-seq readings were searched for the *Odaph* ortholog at either NCBI genome browser (<https://www.ncbi.nlm.nih.gov/>) or Ensemble genome browser (<http://useast.ensembl.org/index.html>).

Results

The *Odaph*^{C41*} dental phenotype. Using the CRISPR/Cas9 system we generated *Odaph*^{C41*} mice in the C57BL/6J background by converting the codon for Cys41 into a translation termination codon. The founders were back-crossed with C57BL/6N wild-type mice for two generations to remove potential off-target effects of the CRISPR/Cas9 editing process. Based upon RT-PCR analyses, the *Odaph*^{C41*} allele appeared to be expressed in both the secretory and maturation stages of amelogenesis, and did not appear to undergo nonsense mediated decay (Fig. S2C). If expressed, the mutant allele would secrete an 18 amino acid peptide: QDVVTPPGGSQN-NAKPTD*, reduced from the 103 amino acids of the wild-type. The dental phenotype was first inspected under a dissecting microscope (Fig. 1). The homozygous *Odaph*^{C41*/C41*} mice could be readily distinguished from their wild-type (*Odaph*^{+/+}) and heterozygous (*Odaph*^{+/C41*}) littermates because of their apparent enamel defects. The incisor enamel was chalky-white and underwent rapid attrition (Fig. 1A,B), despite the animals being fed soft chow. The molar enamel showed a brown discoloration and also underwent rapid attrition (Fig. 1C). The heterozygous *Odaph*^{+/C41*} mice appeared to be normal in all respects.

Timing of *Odaph* expression and pathology. To discern the timing of normal *Odaph* expression and the onset of enamel malformations in *Odaph*^{C41*/C41*} mice, we conducted in situ hybridization studies on sagittally sectioned D12 hemimandibles using custom *Odaph* riboprobes. Developing mandibular incisors display all stages of amelogenesis in a linear array and gave a clear picture of the timing of *Odaph* expression (Fig. 2). Although the positive signal was weak relative to what we have observed for other enamel proteins, it was specific for ameloblasts and showed a clear onset in post-secretory transition and terminated in mid-maturation. No other cells besides ameloblasts were positive. We compared the histology of D12 mandibular incisors from *Odaph*^{+/+} and *Odaph*^{C41*/C41*} mice (Fig. 3). The *Odaph*^{C41*/C41*} incisors appeared to be normal until midway through post-secretory transition. At what should have been the onset of enamel maturation, a cyst formed that separated the ameloblasts from the underlying enamel and flattened the ameloblasts into squamous cells. These events must eliminate the entire maturation process of removing residual enamel protein and hardening the enamel layer by thickening the thin enamel crystals deposited previously during the secretory stage.

We compared the histology of developing maxillary first molars from *Odaph*^{+/+} and *Odaph*^{C41*/C41*} mice at successive stages of development: on D5 (secretory stage), D8 (transition and early maturation) and D12 (late maturation) (Fig. 4). The results were consistent with those for the incisors. Ameloblasts, odontoblasts, dentin and enamel in Day 5 *Odaph*^{C41*/C41*} maxillary molars were indistinguishable from those in the wild-type. On Day 8 cysts were formed on the cusp slopes that expanded the enamel space and flattened the ameloblasts. Root and dentin development appeared to be normal. On D12, polarized maturation ameloblasts were neatly arrayed over the enamel space in the wild-type and only small amounts of residual protein remained in the enamel. In the *Odaph*^{C41*/C41*} molars, flattened epithelial cells lined a cyst-covered enamel space and abundant residual enamel protein remained in the enamel. Although root development progressed similarly in both groups, the mesial root of the *Odaph*^{C41*/C41*} molar was distorted, apparently by pressure from the cyst overlying the adjacent enamel. No apparent pathosis was observed in the surrounding alveolar bone or oral epithelium.

To better visualize the ameloblasts during transition and early maturation, we performed in situ hybridization of *Klk4* mRNA on wild-type and *Odaph*^{C41*/C41*} molars, because *Klk4* has a pattern of expression that closely matches that of *Odaph*^{31–33}, with an identical onset in post-secretory transition (Fig. 5). Specific *Klk4* expression was evident in the flattened cells lining the cysts covering maturation enamel in *Odaph*^{C41*/C41*} molars, supporting the interpretation that the ameloblasts had not died, but had flattened and lined the cysts. The histology strongly suggested that ODAPH was essential for a normal transition from secretory to maturation ameloblasts and potentially for the adhesion of maturation ameloblasts to the enamel surface. In *Odaph*^{C41*/C41*} mice this attachment fails and fluid accumulates in the space between ameloblasts and the enamel surface.

Backscattered scanning electron microscopy. bSEM produces an image like a dental radiograph, with more highly mineralized materials being whiter, and less mineralized materials being grayer. bSEM images of 7-week-old mandibular incisor cross-sections taken at 1 mm increments are a standard means of visualizing the progress of tooth mineralization³⁰. Level 1 through Level 3 corresponds to the secretory stage, while levels 4 through 8 show enamel maturation (Fig. 6). Mineralization of dentin is the same in *Odaph*^{+/+}, *Odaph*^{+/C41*}, and *Odaph*^{C41*/C41*} mice at all stages (Fig. 6, top). In addition, the enamel layer achieves its full thickness and normal contour by Level 3 in all three genotypes. This is very different from the bSEM results when a gene necessary for the secretory stage is affected and the enamel layer fails to expand significantly, as in amelogenin^{34,35}, enamelin³⁶, ameloblastin³⁷, and matrix metalloproteinase 20 (MMP20)^{28,38} null mice.

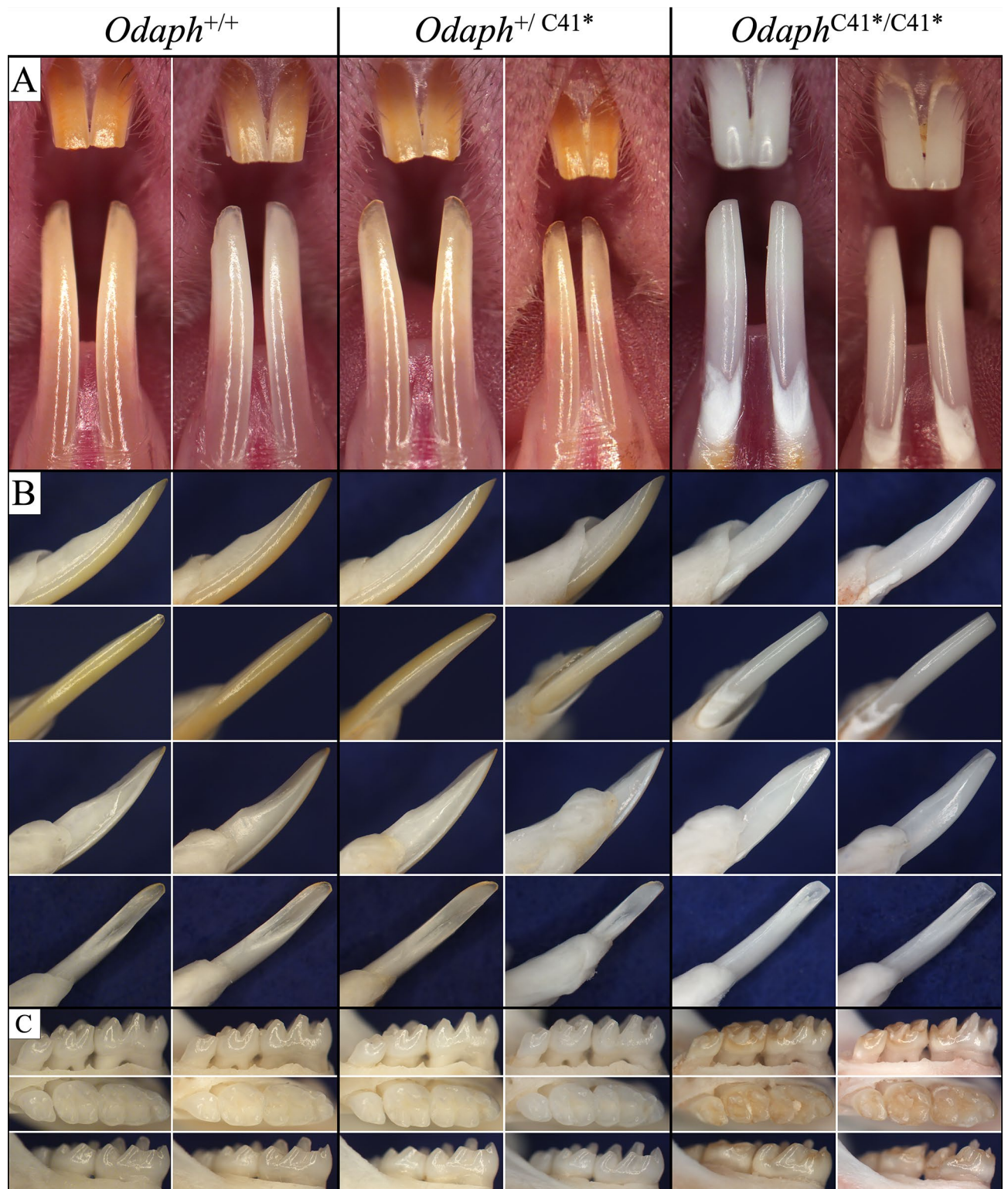


Figure 1. Appearance of *Odaph*^{+/+}, *Odaph*^{+/C41*}, and *Odaph*^{C41*/C41*} Incisors and Molars at 7-weeks. There were no appreciable differences in dental phenotype observed between *Odaph*^{+/+} and *Odaph*^{+/C41*} mice. Tooth size and morphology were similar in the three genotypes. (A) Frontal view of maxillary and mandibular incisors. The *Odaph*^{C41*/C41*} incisors appeared to be severely hypomineralized. Their incisors were chalky white and the enamel had abraded from dentin surface down to the cervical region. (B) Mesial, labial, distal, and lingual (lower right) views of the mandibular incisors. The *Odaph*^{C41*/C41*} incisal edge is flat and appears to be shorter than the wild-type due to attrition. (C) Buccal, Occlusal, and Lingual views of mandibular molars. No differences in alveolar bone level were observed among the three genotypes. The *Odaph*^{C41*/C41*} molars were discolored and had undergone significant attrition.

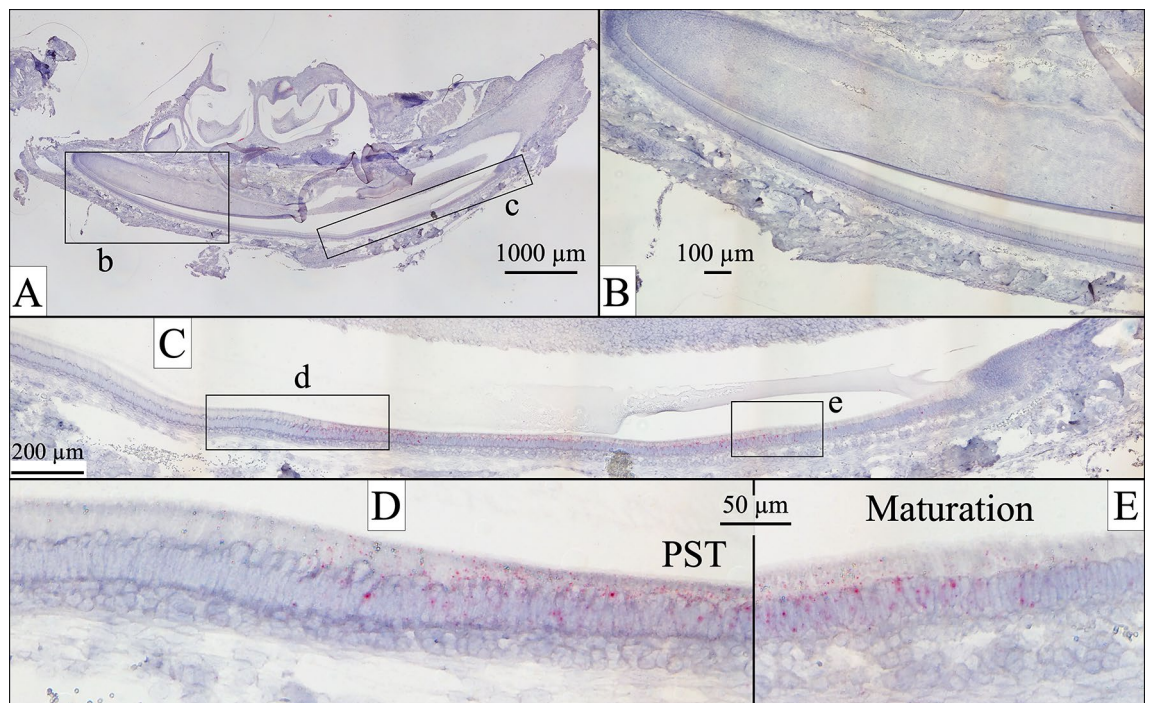


Figure 2. *Odaph* Expression in *Odaph*^{+/+} Day 12 Mandibular Incisors. In the continuously growing mandibular incisor enamel formation progressively advances from basal (left) to incisal (right). (A) Sagittal section of a D12 mouse hemimandible. Boxes show the locations of the higher magnification views in (B) and (C). (B) *Odaph* expression was absent or trace in presecretory and secretory stage ameloblasts. (C) Late secretory, post-secretory transition (PST) and early maturation stages of amelogenesis. Boxes show the locations of the higher magnification views in (D) and (E) *Odaph* expression was low, but could be detected from the middle of box (D) to nearly the end of box (E). (D) On the left the ameloblasts were ending the secretory stage. Approximately midway through image (D), they entered post-secretory transition (PST) where the ameloblasts normally shorten while converting to ruffle-ended maturation stage ameloblasts. Note that *Odaph* expression is observed at the onset of PST. (E). Early maturation ameloblasts were positive for *Odaph* expression. No significant *Odaph* signal was detected in odontoblasts.

The one major difference among the three genotypes is that from Level 4 to Level 8 the enamel layer in *Odaph*^{C41*/C41*} incisors fails to increase in mineral density and remains at the same gray scale, suggesting a complete absence of enamel maturation. This pattern is similar, but somewhat more severe in terms of the reduction in mineral density observed in *Odaph*^{C41*/C41*} maturation stage enamel compared to other mouse knockouts with defects specific to the maturation stage (Fig. S3), such as *Klfa39*³⁹ and *Wdr72*⁴⁰. In addition to the *Odaph*^{C41*/C41*} enamel layer achieving full thickness (but not density), the decussation pattern of enamel rods in the enamel layer was unaffected (Fig. 6, bottom). Enamel defects corresponding to a specific failure of enamel maturation were also observed in the bSEM images of mandibular molars at 7-wks (Fig. 7). The enamel crowns in the molars of all three genotypes showed normal shape and contour (indicative of a normal secretory stage), but the enamel of *Odaph*^{C41*/C41*} was softer and underwent significant attrition compared to the wild-type and *Odaph*^{+/C41*} molars.

Discussion

Odaph expression detected by in situ hybridization was very low in developing mouse teeth. A second riboprobe was ordered and gave the same result. Although the signal was low, it was specific for ameloblasts starting at the onset of ameloblast transition and continuing throughout early maturation stage. As it turned out, the dental phenotype observed in the *Odaph*^{C41*/C41*} knockin mice was entirely consistent with a disturbance in tooth development occurring during the narrow window when *Odaph* was shown to be expressed by in situ hybridization.

A simple inspection of the incisors could distinguish between mice heterozygous (*Odaph*^{+/C41*}) or homozygous (*Odaph*^{C41*/C41*}) for the *Odaph* truncation. Closer histologic examination of developing molars and incisors showed that secretory stage ameloblasts and the forming enamel layer appeared normal in all three genotypes. bSEM analyses showed the *Odaph*^{+/C41*} enamel layer grew to normal thickness and contour, and achieved the same high degree of mineralization and resistance to attrition as the enamel of wild-type mice. The pattern of inheritance of *Odaph* Cys41* mutations in mice is autosomal recessive. This is consistent with the pattern of inheritance in humans and suggests that if the truncated protein had been expressed, it caused no detectable pathosis. Expression of half the normal amount of ODAPH was sufficient for normal amelogenesis in *Odaph*^{+/C41*} mice.

The histology of *Odaph*^{C41*/C41*} molars and incisors showed normal differentiating and secretory stage ameloblasts, but a dramatic failure of ameloblasts to transition normally into the maturation stage. It is apparent that

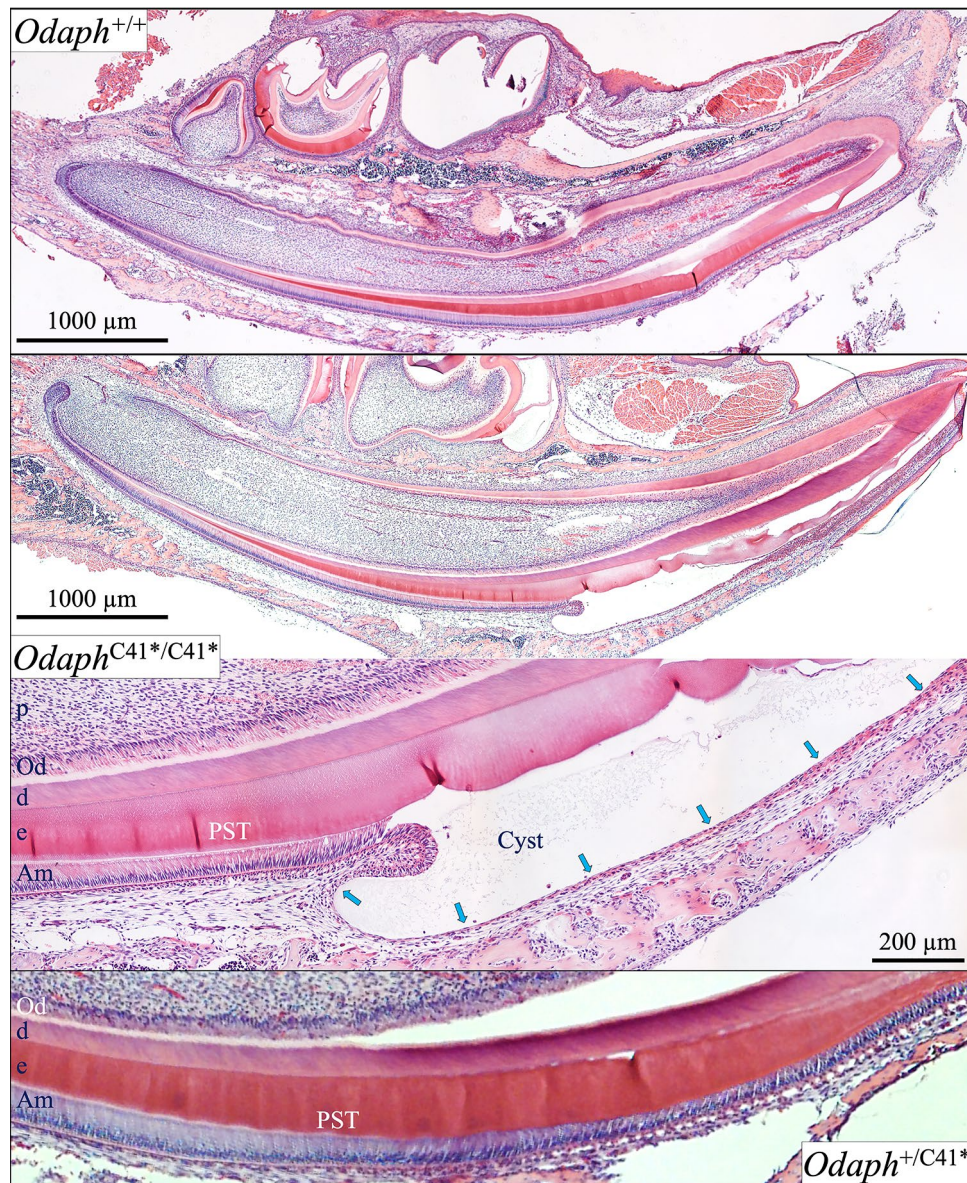


Figure 3. *Odaph*^{+/+}, *Odaph*^{+C41*}, and *Odaph*^{C41*/C41*} Mandibular Incisor Histology at D12. Incisor sagittal sections provide histological information on all stages of enamel formation, including differentiating, presecretory, secretory, transition and maturation ameloblasts. The *Odaph*^{+C41*} incisors (bottom) resembled those of the wild-type (top). The *Odaph*^{C41*/C41*} incisors appeared to be normal until late in post-secretory transition (PST) when ameloblasts abruptly reduced in height and flattened (arrows) at the onset of the maturation when a cyst appeared between the ameloblasts and the enamel surface. Key: p: pulp, Od: odontoblasts, d: dentin, e: enamel, Am: ameloblasts, PST: post secretory transition stage of amelogenesis.

absence of ODAPH during the secretory stage did not impact the enamel rod pattern. This observation did not support the in vitro evidence that ODAPH is required as a nucleator of hydroxyapatite. Dental enamel formation may not require a nucleator (outside of what initiates dentin mineralization), as enamel mineral ribbons initiate on dentin mineral⁴¹ and are subsequently extended and oriented in close proximity to the ameloblast secretory surface^{42–44}. Notably enamelin^{45,46} and ameloblastin⁴⁷, but not amelogenin⁴³, concentrate at the rod and inter-rod membrane growth sites and are absolutely necessary for enamel mineral ribbon initiation and elongation. The elongation of enamel mineral ribbons at a mineralization front along the ameloblast membrane is observed in all cases where true enamel forms, including humans⁴⁴, mouse⁴⁸, lungfish⁴⁸, and gar⁴⁹, and goes back to the origins of enamel during evolution.

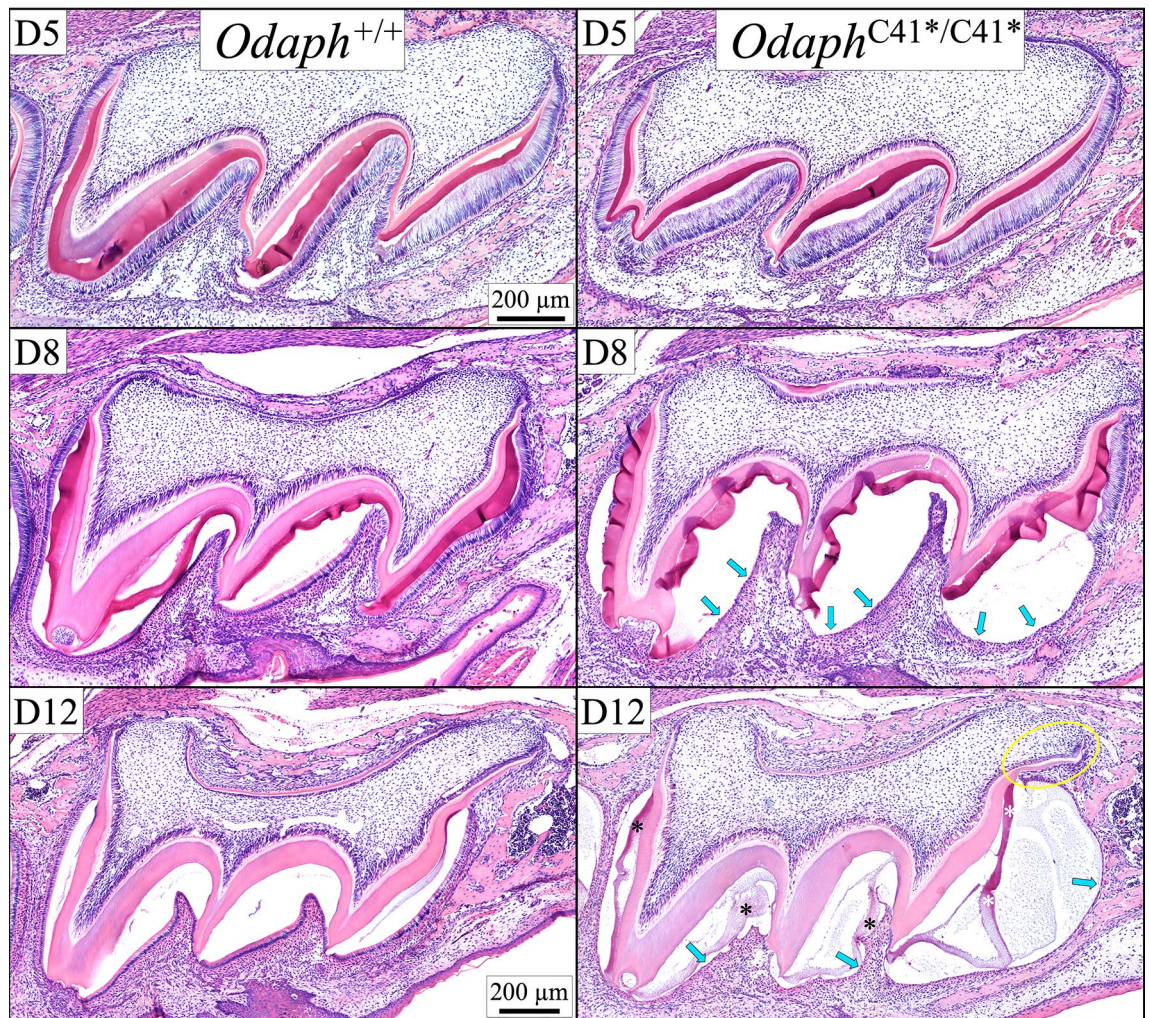


Figure 4. *Odaph*^{+/+} and *Odaph*^{C41*/C41*} Maxillary First Molar Histology at D5, D8 and D12. Day 5 first molar ameloblasts have not yet entered the maturation stage. The histology appearances of *Odaph*^{+/+} and *Odaph*^{C41*/C41*} secretory stage ameloblasts in D5 molars were similar to each other and the degree of enamel and dentin matrix deposition was comparable. Day 8 wild-type first molar ameloblasts are predominantly in the maturation stage. The maturation stage ameloblasts in D8 *Odaph*^{C41*/C41*} molars were flattened along the cuspal slopes (arrows) and the enamel space was expanded, due to apparent cyst formation. Dentin and root development appeared to be normal. On Day 12 molars, polarized late-maturation stage ameloblasts covered the *Odaph*^{+/+} molars, whereas only flattened epithelial cells (arrows) covered the same area in the *Odaph*^{C41*/C41*} molars, and residual enamel matrix (*) was still apparent in the enamel space. Mesial root development was distorted (yellow circle) presumably due to the expanding cystic space at the cervical margin. Dentin, root development, and alveolar bone appeared to be normal.

Gar (*Lepisosteus*) is an actinopterygian, one of the most distant vertebrates from humans that makes enamel^{50,51}. In the gar genome, only *Enam* and *Ambn* genes are found, whereas *Enam*, *Ambn*, and *Amel* are found in coelacanth⁵² and in tetrapods (both clades and lungfish constitute sarcopterygians) that make enamel, suggesting that *Amel* came into existence after the divergence of the common ancestor to gar and coelacanth and after the initial evolution of the enamel mineralization front. Similar to *Enam* and *Ambn*, *Odaph* is found in both sarcopterygians and actinopterygians, implying that *Odaph* is one of the most ancient enamel genes. Unlike mammalian *Odaph*, its non-mammalian orthologs, found in *Alligator*, lizard (*Anolis*), caecilian (*Geotryoetes*), gar, and reedfish (*Erpetoichthys*), consist of three exons and encode a Ser-Ser-Glu-Glu sequence (these two serine residues are potentially phosphorylated) and two or three cysteine residues (one in exon 2 and the other one or two in exon 3). Both introns are phase 1 (the intron is located between the first and the second nucleotides of a codon), confirming that *Odaph* is not a member of the SCPP gene family (all introns are located between two adjacent codons, phase 0). Mammalian *Odaph* genes consist of two exons, which is explained by the deletion of exon 2 in non-mammalian orthologs. One or two Cys and potentially phosphorylated Ser residues encoded by exon 3 of non-mammalian *Odaph* genes are common to most mammalian orthologs, including human *ODAPH*²³.

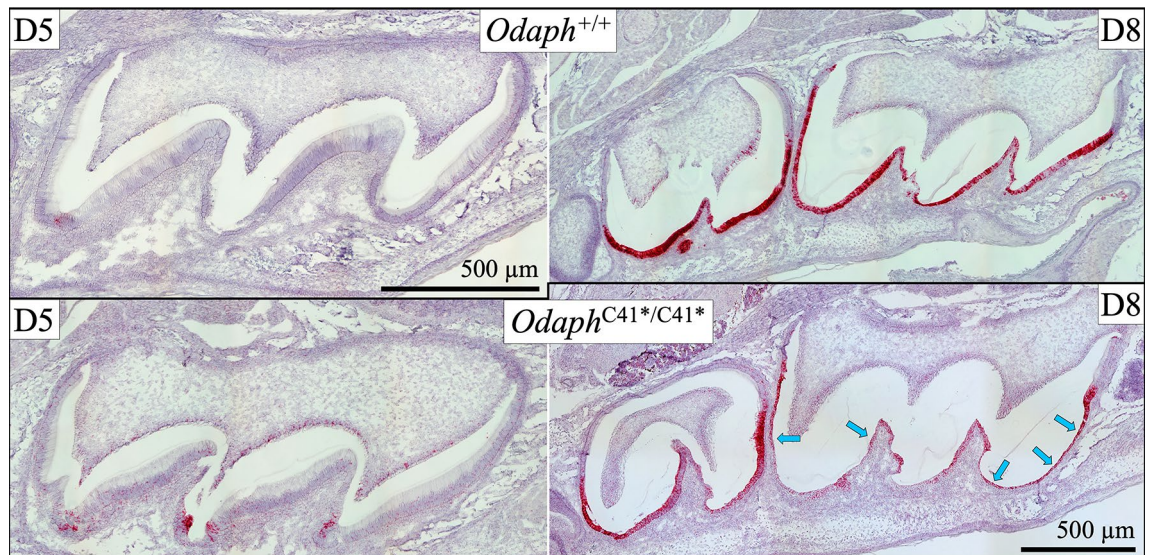


Figure 5. *Klk4* Expression in *Odaph*^{+/+} and *Odaph*^{C41*/C41*} D5 and D8 Maxillary First Molars. On Day 5, positive in situ hybridization for *Klk4* expression was observed in some odontoblasts and in the enamel free zone near the cusp tips of both *Odaph*^{C41*/C41*} and *Odaph*^{+/+} maxillary first molars. On Day 8, after enamel development had progressed into the early maturation stage, positive *Klk4* mRNA signal was specifically observed in transition and maturation ameloblasts of wild-type first and second molars, with spotty signal in odontoblasts. A similar pattern was observed in D8 *Odaph*^{C41*/C41*} maxillary molars but with decreased intensity (arrows) in the flattened ameloblasts lining the expanded, cyst-like enamel space. This *Klk4* expression pattern, although diminished relative to the wild-type, supports the interpretation that the flattened epithelial cells lining the cyst were ameloblasts.

Deviation from normal enamel formation in *Odaph*^{C41*/C41*} mice is evident at the end of ameloblasts' transition into maturation, when ameloblasts lose their columnar shape. A large cyst forms between the enamel and the ameloblasts, which flatten into a squamous morphology. The maturation stage protease *Klk4*, which is normally expressed by ameloblasts at the start of post-secretory transition^{31,53–55}, is expressed by transition ameloblasts in *Odaph*^{C41*/C41*} mice and its expression continues even in the flattened ameloblasts, demonstrating that not all aspects of the transition had failed and that the flattened cells are indeed ameloblasts. In wild-type mice, it is evident during dissections that maturation ameloblasts are *firmly* attached to the enamel layer. Attempting to remove the enamel organ epithelia for the purpose of acquiring soft tissue samples for RT-PCR analyses, invariably results in the shredding of the enamel organ epithelia covering the enamel. This does not normally occur while collecting the soft-tissue covering secretory stage enamel. Consistent formation of a cyst at the onset of maturation in *Odaph*^{C41*/C41*} mice suggests that ODAPH plays a role in cell attachment directly, or indirectly by altering the expression of other genes necessary for attachment. It is also possible that failure of secreted ions to add to crystal surfaces could increase osmotic pressure that causes cyst formation.

Although secretory stage ameloblasts require the expression of the basement-membrane-associated genes *Col17a1*, *Lama3*, *Lamb3*, and *Lamc2*⁵⁶, there is no visible basement membrane beneath secretory stage ameloblasts^{57,58}. During transition and early maturation, in addition to the continued expression of laminin-332^{59–61}, there is the added expression of a panel of novel SCPP genes that contribute to the attachment of maturation stage ameloblasts to the underlying enamel⁶². These genes include *Amtn*^{63,64}, *Odam*⁶³, *Scppp1*⁶⁵ and perhaps *Odaph*. Despite the expression of many basement membrane-derived genes, the attachment of ameloblasts to maturation stage enamel fails completely due to the absence of *Odaph*, a small, low expression, secreted phosphoprotein. Failure of the enamel layer to harden is the most severe that we have observed in any knockout exhibiting hypomaturation enamel specifically, and surpasses the hypomaturation defects displayed by the *Klk4*³⁹ and *Wdr72*⁴⁰ null mice.

The phylogenetic analysis indicates that *Odaph* evolved in reptiles and is present in monotremes, marsupials, and placental mammals. There are significant differences between the dental enamel formed in mammals and reptiles⁶⁶. Mammalian enamel is generally thicker (posing a greater challenge for enamel maturation) and has a rod and interrod organization. The rod and interrod organization is the result of a special modification of the ameloblast distal membrane called the Tomes' process^{67,68} that elongates rod enamel mineral ribbons along the secretory surface of the protruding distal part of the process and interrod enamel mineral ribbons along the proximal part that encircles the cell and includes contributions from adjacent cells^{69,70}. The rod/interrod

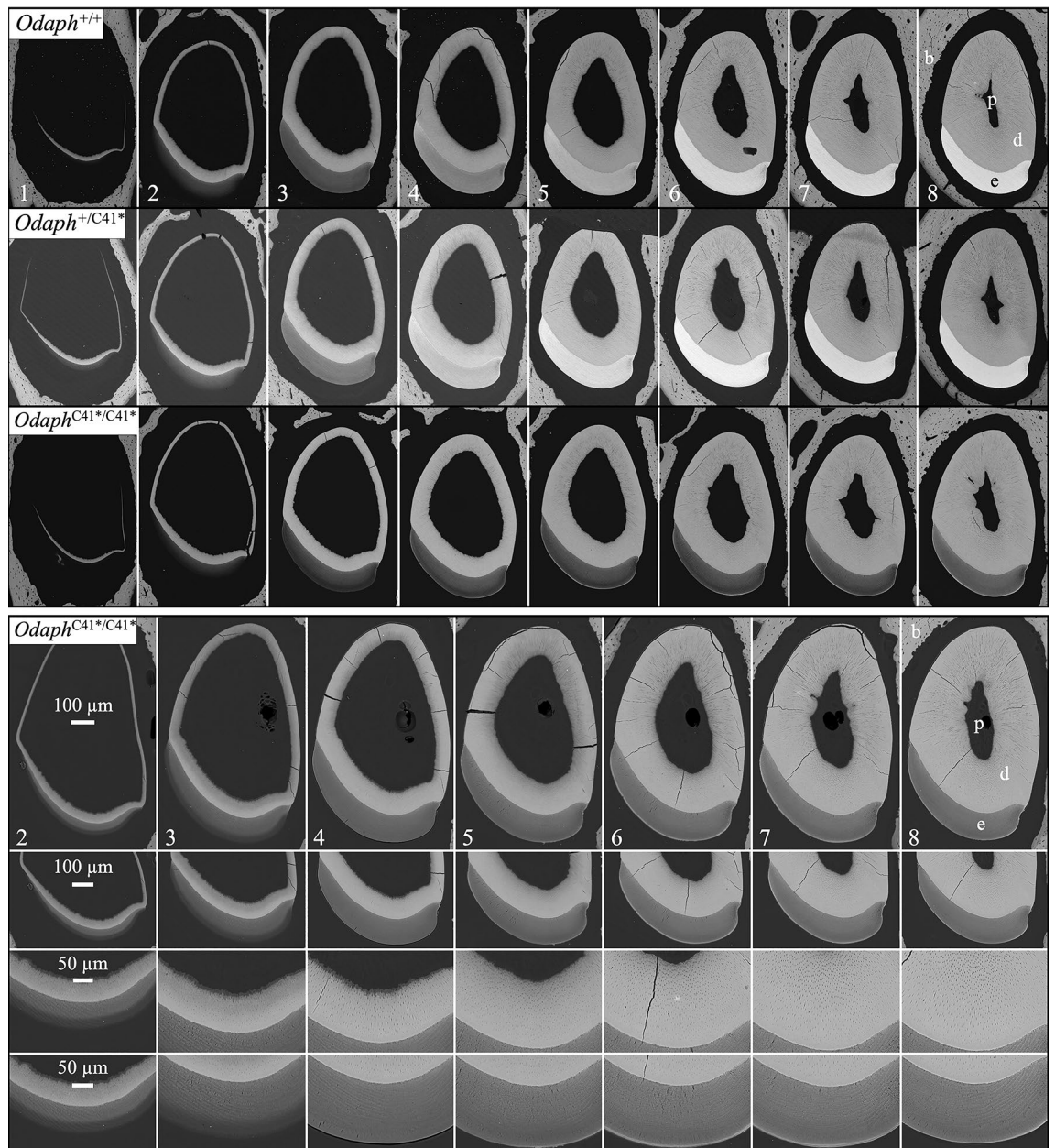


Figure 6. bSEM of 7-wk *Odaph*^{+/+}, *Odaph*^{+/C41*}, and *Odaph*^{C41*/C41*} Mouse Mandibular Incisor Cross-Sections. These panels show 1-mm (basal, left; incisal, right) incremental cross-sections of 7-wk mandibular incisors taken from *Odaph*^{+/+}, *Odaph*^{+/C41*}, and *Odaph*^{C41*/C41*} mice. Top: Comparison of the 3 genotypes from levels 1 to 8 showed that the early progress of dentin and enamel deposition is similar in all three genotypes, with the enamel layer having achieved its final contour and thickness by level 3. After level 3 the striking finding was the failure of the *Odaph*^{C41*/C41*} enamel layer to increase in density, as occurred in the *Odaph*^{+/+} and *Odaph*^{+/C41*} incisors. Bottom: High magnification views of *Odaph*^{C41*/C41*} sections showed normal dentin and dentin tubules and enamel rod decussation patterns and final enamel thickness. The only deficiency was the dramatic lack of enamel maturation in the *Odaph*^{C41*/C41*} incisors. The *Odaph*^{C41*/C41*} enamel surface was the only part of the enamel layer that increased in density. Key: b: bone, p: pulp, d: dentin, e: enamel.

organization of enamel is accomplished before *Odaph* is expressed, but such organization could alter the requirements of cell attachment during the maturation stage. KLK4, a protease that is expressed concurrently with ODAPH, degrades enamel proteins to facilitate their removal from the matrix, evolved even more recently⁷¹ than *Odaph* and is necessary for the maturation of dental enamel in most placental mammals.

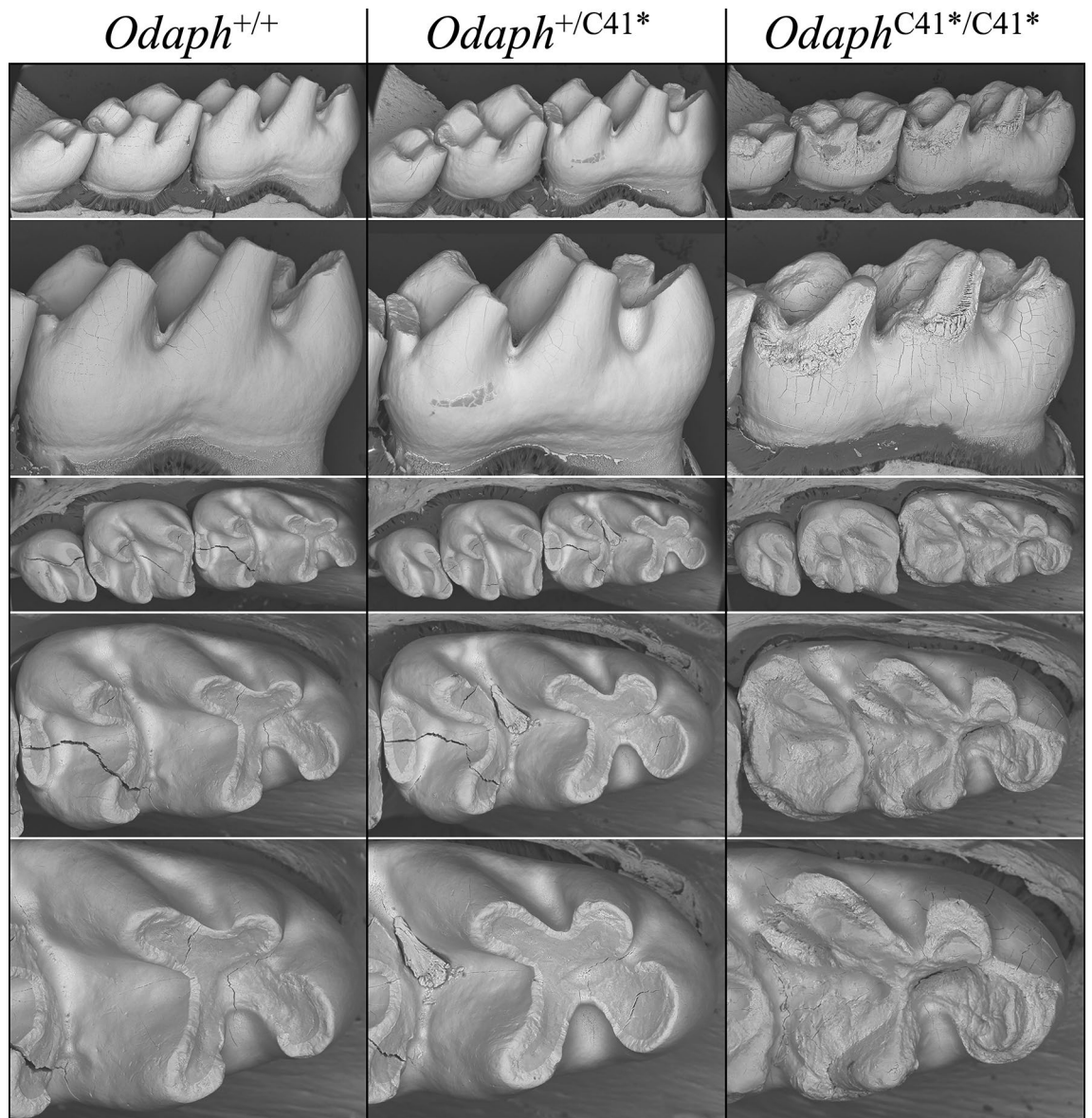


Figure 7. bSEMs of 7-wk *Odaph*^{+/+}, *Odaph*^{+/C41*}, and *Odaph*^{C41*/C41*} Mouse Mandibular First Molars. Lingual (top 2 rows) and occlusal (bottom 3 rows) views of 7-wk mandibular molars. No differences in attrition were observed between *Odaph*^{+/+} and *Odaph*^{+/C41*} molars. The *Odaph*^{C41*/C41*} molars showed extensive attrition. Like the incisors, the molar enamel seemed to reach full thickness but was soft and underwent attrition following eruption.

Received: 14 August 2020; Accepted: 21 December 2020

Published online: 13 January 2021

References

1. Parry, D. A. *et al.* Mutations in C4orf26, encoding a peptide with in vitro hydroxyapatite crystal. *Am. J. Hum. Genet.* **91**, 565–571 (2012).
2. Prasad, M. K., Laouina, S., El Alloussi, M., Dollfus, H. & Bloch-Zupan, A. Amelogenesis imperfecta: 1 family, 2 phenotypes, and 2 mutated genes. *J. Dent. Res.* **95**, 1457–1463 (2016).
3. Springer, M. S. *et al.* Inactivation of C4orf26 in toothless placental mammals. *Mol. Phylogenet. Evol.* **95**, 34–45 (2016).
4. Cui, J. *et al.* A secretory kinase complex regulates extracellular protein phosphorylation. *Elife* **4**, e06120 (2015).
5. O'Sullivan, J. *et al.* Whole-Exome sequencing identifies FAM20A mutations as a cause of amelogenesis imperfecta and gingival hyperplasia syndrome. *Am. J. Hum. Genet.* **88**, 616–620 (2011).
6. Tagliabracci, V. S. *et al.* Secreted kinase phosphorylates extracellular proteins that regulate biomineralization. *Science* **336**, 1150–1153 (2012).
7. Yan, W. J. *et al.* The importance of a potential phosphorylation site in enamelin on enamel formation. *Int. J. Oral Sci.* **9**, e4 (2017).
8. Chan, H. C. *et al.* Altered enamelin phosphorylation site causes amelogenesis imperfecta. *J. Dent. Res.* **89**, 695–699 (2010).
9. Ma, P. *et al.* The importance of serine phosphorylation of ameloblastin on enamel formation. *J. Dent. Res.* **95**, 1408–1414 (2016).

10. Shin, N. Y. *et al.* Amelogenin phosphorylation regulates tooth enamel formation by stabilizing a transient amorphous mineral precursor. *J. Biol. Chem.* **9**, 010506 (2020).
11. Sansom, I. J., Smith, M. P., Armstrong, H. A. & Smith, M. M. Presence of the earliest vertebrate hard tissue in conodonts. *Science* **256**, 1308–1311 (1992).
12. Briggs, D. E. G., Clarkson, E. & Aldridge, R. The conodont animal. *Lethaia* **16**, 1–14 (1983).
13. Donoghue, P. C., Forey, P. L. & Aldridge, R. J. Conodont affinity and chordate phylogeny. *Biol. Rev. Camb. Philos. Soc.* **75**, 191–251 (2000).
14. Murdock, D. J. *et al.* The origin of conodonts and of vertebrate mineralized skeletons. *Nature* **502**, 546–549 (2013).
15. Märss, T. Exoskeletal ultrasculpture of early vertebrates. *J. Vertebr. Paleontol.* **26**, 235–252 (2006).
16. Žigaitė, Z., Richter, M., Karatajūtė-Talimaa, V. & Meredith Smith, M. Tissue diversity and evolutionary trends of the dermal skeleton of Silurian thelodonts. *Hist. Biol.* **25**, 143–154 (2013).
17. Vaškaninová, V. *et al.* Marginal dentition and multiple dermal jawbones as the ancestral condition of jawed vertebrates. *Science* **369**, 211–216 (2020).
18. Kawasaki, K. & Weiss, K. M. Mineralized tissue and vertebrate evolution: the secretory calcium-binding phosphoprotein gene cluster. *Proc. Natl. Acad. Sci. U.S.A.* **100**, 4060–4065 (2003).
19. Kawasaki, K., Suzuki, T. & Weiss, K. M. Genetic basis for the evolution of vertebrate mineralized tissue. *Proc. Natl. Acad. Sci. U.S.A.* **101**, 11356–11361 (2004).
20. Salido, E. C., Yen, P. H., Koprivnikar, K., Yu, L. C. & Shapiro, L. J. The human enamel protein gene amelogenin is expressed from both the X and the Y chromosomes. *Am. J. Hum. Genet.* **50**, 303–316 (1992).
21. Kawasaki, K., Buchanan, A. V. & Weiss, K. M. Biomineralization in humans: making the hard choices in life. *Annu. Rev. Genet.* **43**, 119–142 (2009).
22. Simmer, J. P. *et al.* Regulation of dental enamel shape and hardness. *J. Dent. Res.* **89**, 1024–1038 (2010).
23. Smith, C. E. Cellular and chemical events during enamel maturation. *Crit. Rev. Oral Biol. Med.* **9**, 128–161 (1998).
24. Nanci, A. in *Ten Cate's Oral Histology Development, Structure, and Function* (ed A Nanci) 141–190 (Mosby, 2008).
25. Hafstrom-Bjorkman, U., Sundstrom, F. & ten Bosch, J. J. Fluorescence in dissolved fractions of human enamel. *Acta Odontol. Scand.* **49**, 133–138 (1991).
26. Wang, S. K. *et al.* The enamel phenotype in homozygous Fam83h truncation mice. *Mol. Genet. Genomic Med.* **7**, e724 (2019).
27. Kim, J. W. *et al.* Mutations in RELT cause autosomal recessive amelogenesis imperfecta. *Clin. Genet.* **95**, 375–383 (2019).
28. Hu, Y. *et al.* MMP20, KLK4, and MMP20/KLK4 double null mice define roles for matrix proteases during dental enamel formation. *Mol. Genet. Genomic Med.* **4**, 178–196 (2016).
29. Smith, C. E. *et al.* Relationships between protein and mineral during enamel development in normal and genetically altered mice. *Eur. J. Oral Sci.* **119**(Suppl 1), 125–135 (2011).
30. Hu, Y., Hu, J. C., Smith, C. E., Bartlett, J. D. & Simmer, J. P. Kallikrein-related peptidase 4, matrix metalloproteinase 20, and the maturation of murine and porcine enamel. *Eur. J. Oral Sci.* **119**, 217–225 (2011).
31. Simmer, J. P., Hu, Y., Richardson, A. S., Bartlett, J. D. & Hu, J. C. Why does enamel in Klk4-null mice break above the dentino-enamel junction? *Cells Tissues Organs* **194**, 211–215 (2011).
32. Simmer, J. P. & Hu, J. C. Expression, structure, and function of enamel proteinases. *Connect. Tissue Res.* **43**, 441–449 (2002).
33. Simmer, J. P., Richardson, A. S., Smith, C. E., Hu, Y. & Hu, J. C. Expression of kallikrein-related peptidase 4 in dental and non-dental tissues. *Eur. J. Oral Sci.* **119**(Suppl 1), 226–233 (2011).
34. Hu, Y. *et al.* Enamel ribbons, surface nodules, and octacalcium phosphate in C57BL/6 Amelx^{-/-} mice and Amelx^{+/-} lyonization. *Mol. Genet. Genomic Med.* **4**, 641–661 (2016).
35. Gibson, C. W. *et al.* Amelogenin-deficient mice display an amelogenesis imperfecta phenotype. *J. Biol. Chem.* **276**, 31871–31875 (2001).
36. Hu, J. C. *et al.* Enamel defects and ameloblast-specific expression in Enam knock-out/lacZ knock-in mice. *J. Biol. Chem.* **283**, 10858–10871 (2008).
37. Liang, T. *et al.* AMBN mutations causing hypoplastic amelogenesis imperfecta and Ambn knockout-NLS-lacZ knockin mice exhibiting failed amelogenesis and Ambn tissue-specificity. *Mol. Genet. Genomic Med.* **7**, e929 (2019).
38. Caterina, J. J. *et al.* Enamelysin (matrix metalloproteinase 20)-deficient mice display an amelogenesis imperfecta phenotype. *J. Biol. Chem.* **277**, 49598–49604 (2002).
39. Simmer, J. P., Hu, Y., Lertlam, R., Yamakoshi, Y. & Hu, J. C. Hypomaturation enamel defects in Klk4 knockout/LacZ knockin mice. *J. Biol. Chem.* **284**, 19110–19121 (2009).
40. Wang, S.-K. *et al.* Critical roles for WDR72 in calcium transport and matrix protein removal during enamel maturation. *Mol. Genet. Genomic Med.* **3**, 302–319 (2015).
41. Smith, C. E., Hu, Y., Hu, J. C. & Simmer, J. P. Ultrastructure of early amelogenesis in wild-type, Amelx^{-/-}, and Enam^{-/-} mice: enamel ribbon initiation on dentin mineral and ribbon orientation by ameloblasts. *Mol. Genet. Genomic Med.* **4**, 662–683 (2016).
42. Simmer, J. P., Richardson, A. S., Hu, Y. Y., Smith, C. E. & Hu, J. C.-C. A post-classical theory of enamel biomineralization... and why we need one. *Int. J. Oral Sci.* **4**, 129–134 (2012).
43. Nanci, A., Hashimoto, J., Zalzal, S. & Smith, C. E. Transient accumulation of proteins at interdental and rod enamel growth sites. *Adv. Dent. Res.* **10**, 135–149 (1996).
44. Ronnholm, E. The amelogenesis of human teeth as revealed by electron microscopy II The development of the enamel crystallites. *J. Ultrastructure Res.* **6**, 249–303 (1962).
45. Hu, C. C. *et al.* Cloning and characterization of porcine enamelin mRNAs. *J. Dent. Res.* **76**, 1720–1729 (1997).
46. Uchida, T., Tanabe, T., Fukae, M. & Shimizu, M. Immunocytochemical and immunochemical detection of a 32 kDa nonamelogenin and related proteins in porcine tooth germs. *Arch. Histol. Cytol.* **54**, 527–538 (1991).
47. Nanci, A. *et al.* Protein synthesis by ameloblasts and selective accumulation of some nonamelogenins at enamel growth sites. *Connect. Tis. Res.* **39**, 1–2 (1998).
48. Satchell, P. G., Shuler, C. F. & Diekwisch, T. G. True enamel covering in teeth of the Australian lungfish *Neoceratodus forsteri*. *Cell Tissue Res.* **299**, 27–37 (2000).
49. Sire, J. Y. Light and TEM study of nonregenerated and experimentally regenerated scales of *Lepisosteus oculatus* (Holostei) with particular attention to ganoine formation. *Anat. Rec.* **240**, 189–207 (1994).
50. Sire, J. Y., Delgado, S. & Girondot, M. The amelogenin story: origin and evolution. *Eur. J. Oral Sci.* **114**(Suppl 1), 64–77 (2006).
51. Sire, J. Y., Davit-Beal, T., Delgado, S. & Gu, X. The origin and evolution of enamel mineralization genes. *Cells Tissues Organs* **186**, 25–48 (2007).
52. Kawasaki, K. & Amemiya, C. T. SCPP genes in the coelacanth: tissue mineralization genes shared by sarcopterygians. *J. Exp. Zool. B Mol. Dev. Evol.* **322**, 390–402 (2014).
53. Hu, J. C. *et al.* Localization of EMSP1 expression during tooth formation and cloning of mouse cDNA. *J. Dent. Res.* **79**, 70–76 (2000).
54. Hu, J. C. *et al.* Enamelysin and kallikrein-4 mRNA expression in developing mouse molars. *Eur. J. Oral Sci.* **110**, 307–315 (2002).
55. Hu, J. C.-C. *et al.* Enamelysin and kallikrein-4 expression in developing mouse molars. *Eur. J. Oral Sci.* **110**, 307–315 (2002).
56. Smith, C. E. L. *et al.* Amelogenesis imperfecta; genes, proteins, and pathways. *Front. Physiol.* **8**, 435 (2017).
57. Reith, E. J. The early stage of amelogenesis as observed in molar teeth of young rats. *J. Ultrastruct. Res.* **17**, 503–526 (1967).

58. Kallenbach, E. Electron microscopy of the differentiating rat incisor ameloblast. *J. Ultrastruct. Res.* **35**, 508–531 (1971).
59. Sawada, T. Ultrastructural and immunocytochemical characterization of ameloblast-enamel adhesion at maturation stage in amelogenesis in *Macaca fuscata* tooth germ. *Histochem. Cell. Biol.* **144**, 587–596 (2015).
60. Sahlberg, C., Hormia, M., Airenne, T. & Thesleff, I. Laminin gamma2 expression is developmentally regulated during murine tooth morphogenesis and is intense in ameloblasts. *J Dent Res* **77**, 1589–1596 (1998).
61. Hormia, M., Sahlberg, C., Thesleff, I. & Airenne, T. The epithelium-tooth interface—a basal lamina rich in laminin-5 and lacking other known laminin isoforms. *J. Dent. Res.* **77**, 1479–1485 (1998).
62. Fouillen, A. *et al.* Interactions of AMTN, ODAM and SCPPPQ1 proteins of a specialized basal lamina that attaches epithelial cells to tooth mineral. *Sci. Rep.* **7**, 46683. <https://doi.org/10.1038/srep46683> (2017).
63. Dos Santos Neves, J. *et al.* Odontogenic ameloblast-associated and amelotin are novel basal lamina components. *Histochem. Cell. Biol.* **137**, 329–338 (2012).
64. Moffatt, P. *et al.* Cloning of rat amelotin and localization of the protein to the basal lamina of maturation stage ameloblasts and junctional epithelium. *Biochem. J.* **399**, 37–46 (2006).
65. Moffatt, P., Wazen, R. M., Dos Santos Neves, J. & Nanci, A. Characterisation of secretory calcium-binding phosphoprotein-proline-glutamine-rich 1: a novel basal lamina component expressed at cell-tooth interfaces. *Cell Tissue Res.* **358**, 843–855 (2014).
66. Sander, P. in *Development, Function and Evolution of Teeth* (eds M.F. Teaford, M.M. Smith, & M.W.J. Ferguson) Ch. 7, 92–106 (Cambridge University Press, 2000).
67. Tomes, J. On the structure of the dental tissues of marsupial animals, and more especially of the enamel. *Philos. Trans. R. Soc. Lond.* **139**, 403–412 (1849).
68. Tomes, J. On the structure of the dental tissues of the order rodentia. *Philos. Trans. R. Soc. Lond.* **140**, 529–567 (1850).
69. Nanci, A. & Warshawsky, H. Characterization of putative secretory sites on ameloblasts of the rat incisor. *Am. J. Anat.* **171**, 163–189 (1984).
70. Skobe, Z. The secretory stage of amelogenesis in rat mandibular incisor teeth observed by scanning electron microscopy. *Calcif. Tissue Res.* **21**, 83–103 (1976).
71. Kawasaki, K., Hu, J. C. & Simmer, J. P. Evolution of Klk4 and enamel maturation in eutherians. *Biol. Chem.* **395**, 1003–1013 (2014).

Acknowledgements

This study was funded by the research Grant UG3DE028849 (JC-CH) and R01DE027675 (JPS) from NIDCR/NIH. National Science Foundation (Grants BCS0725227 and BCS0343442 to KK). We acknowledge the Transgenic Animal Model Core of the University of Michigan's Biomedical Research Core Facilities for their generous and expert help in generating and validating the knockin mouse.

Author contributions

T.L., J.P.S., and J.C.-C.H. contributed to the design of the research. C.Z., H.Z., Y.H., K.K., T.L.S., and T.L. performed the research and contributed to the obtained results. K.K. performed the phylogenetic analysis. T.L.S. designed the strategy and oversaw the generation of the Crispr mice. Y.H. was responsible for processing animals and preparing the blocks used for bSEM imaging. C.Z. compiled photo images of the mice and H.Z. conducted RT-PCR and genotyping experiments. J.C.-C.H., and J.P.S. supervised the project. J.C.-C.H. and J.P.S. wrote the manuscript, prepared it for publication, and take responsibility for the integrity of the data and analyses. All authors read and approved the final manuscript submitted for review.

Competing interests

The authors declare no competing interests.

Additional information

Supplementary Information The online version contains supplementary material available at <https://doi.org/10.1038/s41598-020-80912-y>.

Correspondence and requests for materials should be addressed to J.P.S.

Reprints and permissions information is available at www.nature.com/reprints.

Publisher's note Springer Nature remains neutral with regard to jurisdictional claims in published maps and institutional affiliations.



Open Access This article is licensed under a Creative Commons Attribution 4.0 International License, which permits use, sharing, adaptation, distribution and reproduction in any medium or format, as long as you give appropriate credit to the original author(s) and the source, provide a link to the Creative Commons licence, and indicate if changes were made. The images or other third party material in this article are included in the article's Creative Commons licence, unless indicated otherwise in a credit line to the material. If material is not included in the article's Creative Commons licence and your intended use is not permitted by statutory regulation or exceeds the permitted use, you will need to obtain permission directly from the copyright holder. To view a copy of this licence, visit <http://creativecommons.org/licenses/by/4.0/>.

© The Author(s) 2021